J. Fluid Mech. (1994), *vol.* 259, *pp.* 281–290

Small-scale structure in colliding off-axis vortex rings

By G. B. SMITH AND T. WEI

Department of Mechanical and Aerospace Engineering, Rutgers University, Piscataway, NJ 08855-0909, USA

(Received 4 August 1992 and in revised form 14 June 1993)

Off-axis collisions of equal-strength vortex rings were experimentally examined. Two equal-strength vortices were generated which moved toward each other along parallel, but offset, trajectories. Two colour laser-induced fluorescence visualization techniques were used to observe these phenomena and gain insight into their importance in vortex interactions. The most prominent features of this interaction were rapid growth and rotation of the rings and formation of evenly spaced ringlets around the cores of the original rings. Large-scale motions are described using simple vortex induction arguments. The small scales are caused by nonlinear amplification of instabilities during the asymmetric interaction.

1. Introduction

Studies of vortex ring collisions, both with a solid boundary and with other rings, have provided a wealth of information about vortex dynamics. The fascinating feature of all of these collisions is the amazing complexity resulting from nominally simple initial conditions. What appears to the naked eye as virtually instantaneous transition to turbulence is actually an evolution of small, rapidly evolving, highly coherent structures. This is a report on the collision of two equal-strength vortex rings initially propagating toward one another along parallel, but offset, axes.

This problem has been examined numerically by Zawadzki & Aref (1991). An end-view schematic of the interaction appears in figure 1. In the drawing, the black ring moves perpendicularly out of the page and the grey ring propagates along a normal into the page. Note that the two rings are offset horizontally.

Zawadzki & Aref (1991) used vortex-in-cell methods to determine large-scale motions of the vortices. They observed a significant increase in ring radii accompanied by rotation of the interacting rings. The increase in ring radii was due to mutual induction of the interacting rings. Zawadzki & Aref (1991) explained the rotation as conservation of angular impulse. They did not observe generation of small scales.

Lim & Nickels (1992) recently published an impressive set of dye visualization photographs showing a head-on collision of equal-strength vortex rings. The Reynolds number of the rings was ~ 1000 based on ring diameter and initial velocity. In their photographs, Lim & Nickels (1992) showed the formation of tiny rings which move radially away from the symmetry axis of the original rings. These tiny rings were end products of vortex reconnection following excitation of the Crow instability in two anti-parallel vortex rings.

There is still much to be learned from studying off-axis vortex ring collisions. At the time of writing, no published experimental papers have been found. In this paper, results of a controlled experimental study of off-axis vortex ring collisions are

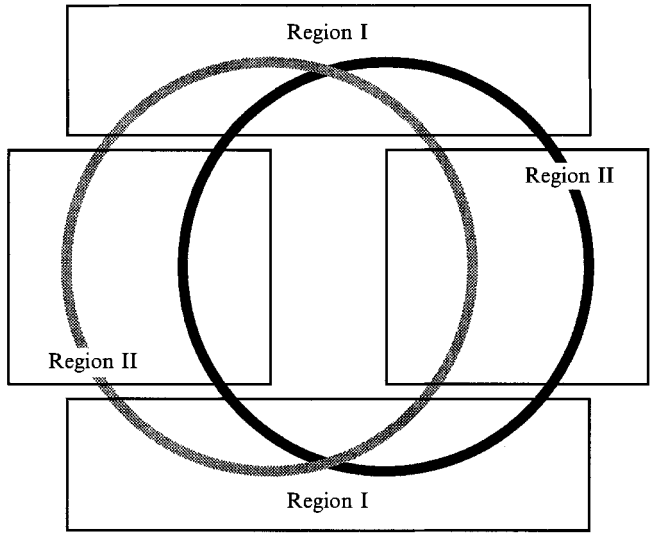

FIGURE 1. End-view schematic showing the off-axis collision of equal-strength vortex rings. The black ring moves directly out of the page while the grey ring propagates normally inward.

presented. The objectives of this work are to identify small-scale structures arising during off-axis vortex ring collisions, and to gain insight into how these structures contribute to turbulence decay.

2. Experimental methods

Experiments were conducted in the test section of a large free-surface water tunnel. The test section was constructed entirely of glass and measured 609.6 cm in length, 58.42 cm in width, and 121.92 cm in depth. In these experiments, the water was quiescent.

Laser-induced fluorescence (LIF) flow visualization techniques were used to visually observe the flow. A 4 W argon-ion laser was used to illuminate the flow. Light sheets were produced by sweeping the laser beam with a General Scanning G112 galvanometer driven by a sawtooth waveform from a function generator. Video records were made using a professional $\frac{3}{4}$ in. video system. Details of the visualization geometries are presented in the following section.

2.1. *Flow visualization*

Two nominally equal-strength vortex rings were generated which travelled toward each other along parallel but offset paths. The vortex generators constructed for this experiment were spring-driven pistons that displaced water past a sharp-edged orifice. They were constructed from 36.2 cm lengths of Plexiglas tube with 10.16 cm inner diameters. The front end of each tube was fitted with a 7.62 cm diameter sharp-edged orifice. Top and side view schematics of the generators and their placement are shown in figure 2.

Great care was taken to ensure that the generators were both level and parallel to the test section sidewalls. The separation distance between orifices was 27.94 cm, and the offset in the horizontal plane, δ, was 2.54 cm. This corresponded to approximately 40% of the ring radius. There was no vertical offset.

In the flow visualization experiments, three different viewing orientations were used.

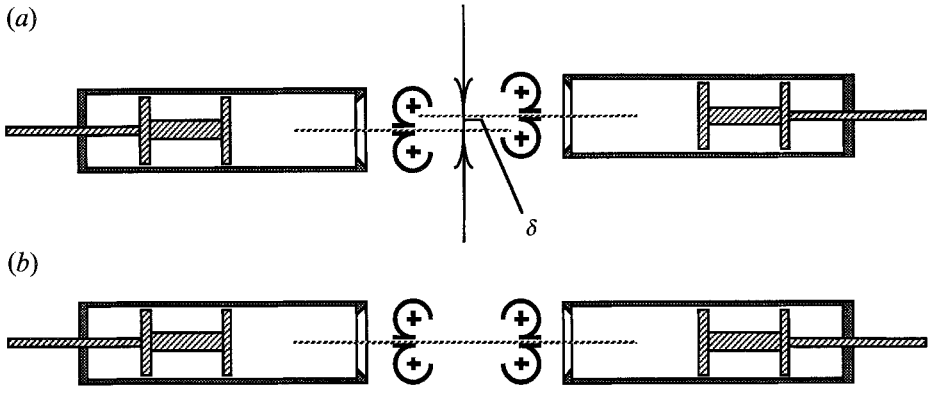

FIGURE 2. (*a*) Top- and (*b*) side-view schematics showing the positioning of the two vortex generators.

Top-view visualizations were done using a horizontal laser sheet placed at the midplane of the vortex generators, as illustrated in figure 2(*a*). Side views were obtained by placing a vertical laser sheet parallel to and between the two vortex ring axes of symmetry, as represented in figure 2(*b*). The third view also employed a vertical laser sheet, but the vertical sheet was placed at $\sim 45°$ to the vortex ring paths (as opposed to perpendicular to the ring paths). This was done to capture structures that formed as the colliding rings rotated. This will be described in greater detail in §3.

Vortices were marked by filling the vortex generators with dilute dye solutions (< 1 p.p.m. by weight). Fluorescein was placed in one generator and rhodamine was placed in the other. Sufficient time was allowed for the water to come to rest before generating the vortices. This was determined by watching the motion of residual dye and particles illuminated by the laser sheet.

2.2. *Vortex ring characteristics*

Over forty experimental runs were made in this study at a nominal Reynolds number of ~ 7500 based on ring diameter and propagation speed. This is in addition to over one hundred runs conducted by Smith & Wei (1991) using a different apparatus. The phenomena described in §3 were reproducible as long as the two rings were of approximately equal strength.

While vortex diameters were reproducible to within 2%, ring velocities were found to vary between generators. The mean Reynolds number from one generator was 7750 with maximum deviations from the mean of $\pm 5\%$. The second generator produced vortices with mean Reynolds number of 6980 and maximum deviations from the mean of $\pm 40\%$. It was therefore necessary to constantly monitor the motion of the second piston. In each collision experiment, the Reynolds numbers of the two rings were measured and compared. If Reynolds numbers differed by more than 10%, the video record was not used.

3. Results and discussion

3.1. *Large-scale features*

Before examining the photographs, it would be instructive to consider what would be the large-scale motions in off-axis ring collisions. When two rings are far apart, they travel under their own self-induction; the influence of the opposing ring is minimal. As

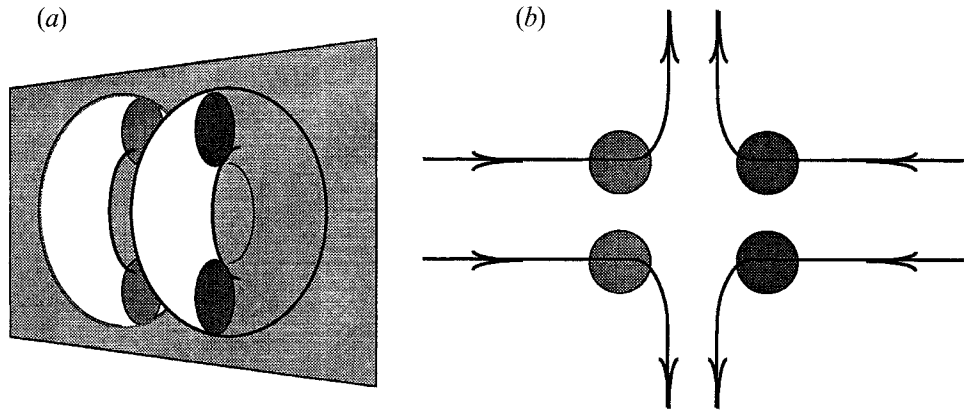

FIGURE 3. (*a*) Oblique and (*b*) orthographic drawings of the side-view visualization orientation. Arrows in (*b*) indicate trajectories of the vortex elements illuminated by a vertical light sheet.

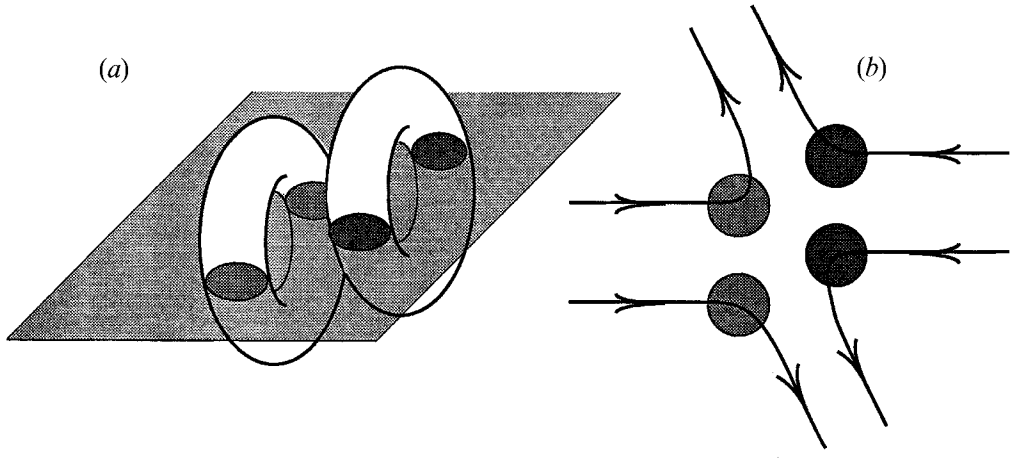

FIGURE 4. (*a*) Oblique and (*b*) orthographic drawings of the top-view visualization orientation. Arrows in (*b*) indicate trajectories of the vortex elements illuminated by a horizontal light sheet.

the two rings draw near, the influence of the opposing ring will dominate. In an axisymmetric collision, forward motions of the rings stop and the two rings expand axisymmetrically.

For an off-axis collision, a similar expansion would be expected. However, one should not expect axisymmetric expansion. Figures 3 and 4 are schematic drawings illustrating the motions that would be observed in vertical and horizontal cross-sections of the collision. Figure 3(*a*) is an oblique sketch showing two rings illuminated by a vertical laser sheet aligned parallel to the vortex trajectories and positioned midway between the two axes. In this view, the collision should appear as a symmetric interaction of four equal-strength vortices. Figure 3(*b*) is an orthographic projection showing the vortex motions in the illuminated plane. As in the true axisymmetric case, the 'upper right' vortex would appear to pair with the 'upper left' and move upward. Simultaneously, the 'lower right' vortex would pair with the 'lower left' and move downward.

When viewed from above, asymmetry would become readily apparent. Figure 4(*a*) shows the same two vortex rings illuminated by a horizontal laser light sheet positioned at the midplane of the rings. Figure 4(*b*) is an orthographic projection of the

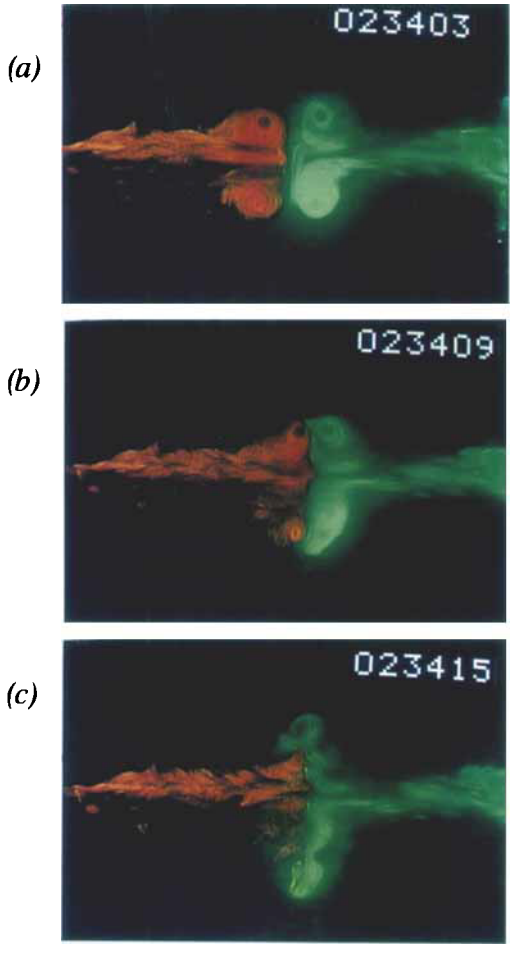

FIGURE 5. Side-view LIF sequence showing off-axis collision of equal-strength vortex rings. The Reynolds numbers of the left and right rings are 7750 and 7015, respectively. Time between successive photographs is 0.1 s.

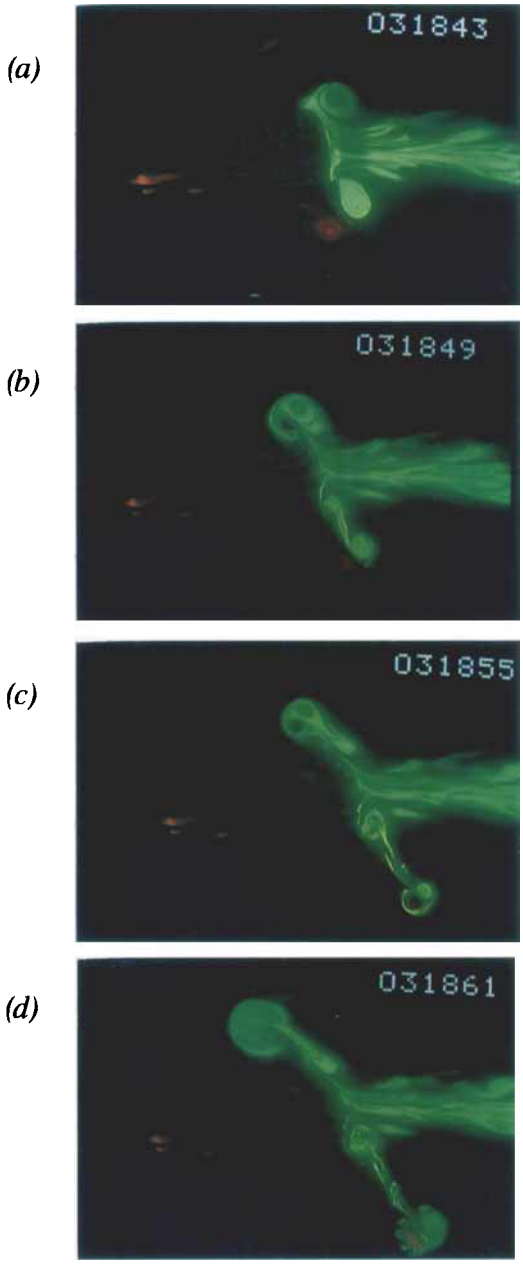

FIGURE 6. Top-view LIF sequence showing asymmetric nature of the collision. The Reynolds numbers of the left and right rings are 7610 and 6773, respectively. Time between successive photographs is 0.1 s.

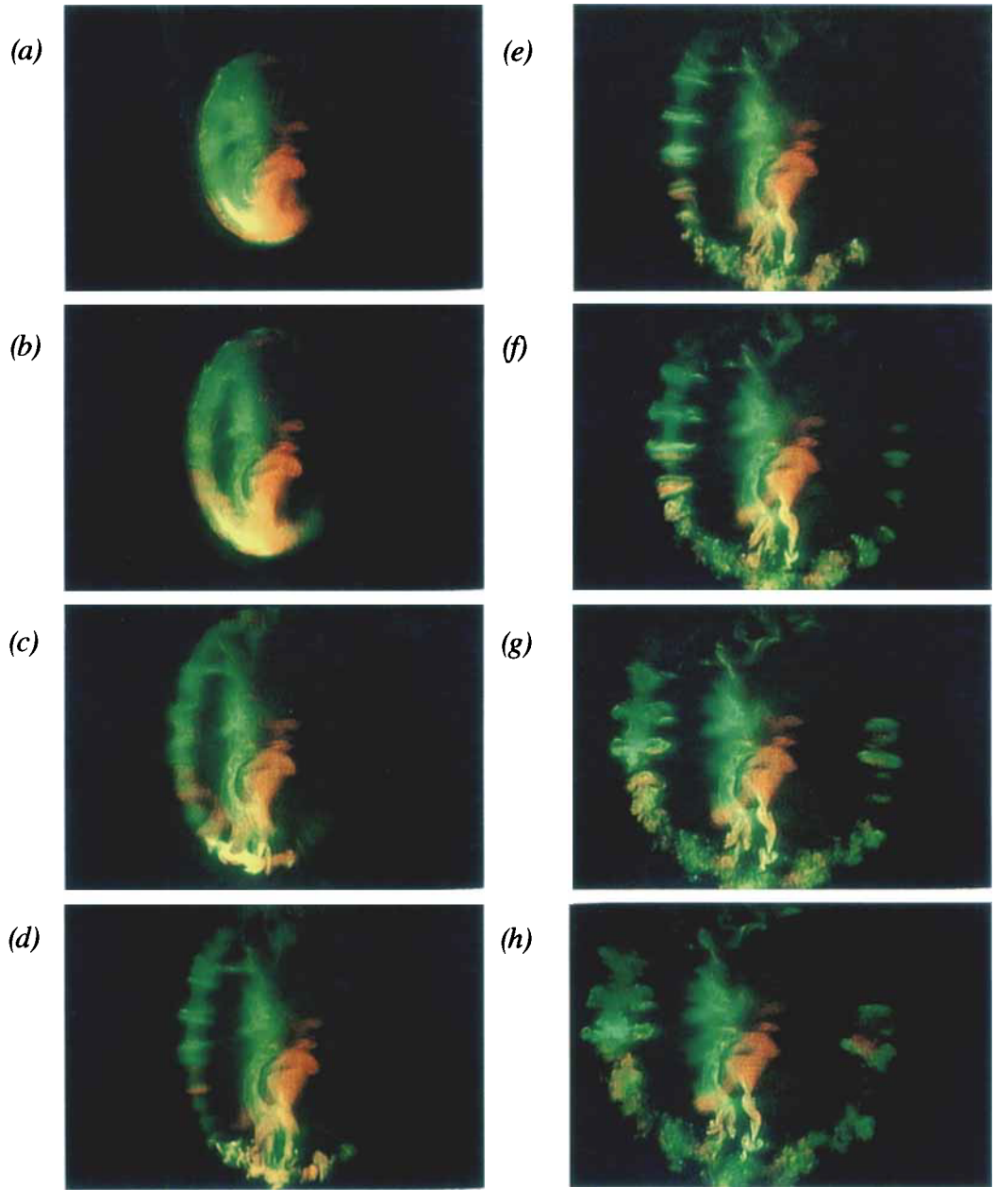

FIGURE 8. Oblique-view LIF sequence showing formation of small-scale ringlets. The Reynolds numbers of the rings were nominally 9300. Time between successive photographs is 0.05 s.

illuminated vortex elements. In this view, the right vortex ring, marked as the darker shaded circles, is shifted up relative to the lighter shaded left ring. The 'upper right' vortex element still pairs with the 'upper left' but the resulting motion is up and to the left (and not purely vertically upward as in the symmetric collision). In the same way, the 'lower right' element pairs with the 'lower left' and moves down and to the right.

Taken *in toto*, off-axis collisions of equal-strength vortex rings result in expansion and rotation of the original rings. This was observed in the present experiments and by Zawadzki & Aref (1991). Representative side- and top-view photographic sequences, taken from video segments, are shown in figures 5 and 6, respectively. The time between successive photographs in both sequences is 0.20 s.

A note on the experiments needs to be interjected at this point. Radiation from fluorescein dye (green) was observed to be much stronger than light radiated by rhodamine dye (red). Consequently, when fluid elements marked with the two different dyes came together, the red pigment was often rendered invisible by the green. One must therefore be careful not to assume, based on colours observed, that red fluid is absent in a photograph.

Figure 5 (plate 1) is a three-photograph sequence showing symmetry in the side view. Reynolds numbers of the left (red) and right (green) rings were 7750 and 7015, respectively. The sequence begins, figure 5(*a*), shortly before the rings collide. Successive photographs, figures 5(*b*) and 5(*c*), show the expansion of the two rings. Note the symmetry in this view. As the ring diameters increase, the cores shrink and turbulence is generated. This is better seen in other views.

A sequence of four top-view photographs appears in figure 6 (plate 1). This is the view corresponding to the schematics shown in figure 4. In this run, the Reynolds numbers of the left and right vortices were 7610 and 6773, respectively. This view clearly shows rotation of the rings associated with asymmetric collisions. Figure 6(*a*) shows two rings very early in the collision. With successive time steps, vortex elements in the upper half of the photographs pair and move up and to the left. Similarly, elements in the lower half-lane move down and to the right. In this sequence, reduction in core diameters is evident.

A fascinating feature of figure 6(*d*) is the evenly spaced small scales around the lower right-hand corner vortex 'pair'. The vortices take on the appearance of a circular saw blade. These features may be related to very repeatable small scales observed in oblique view sequences.

3.2. *Small-scale features*

Observation of small scales required an additional viewing orientation. A vertical laser sheet was placed $\sim 45°$ to the original vortex trajectories. Relative to figure 6, the sheet passed perpendicularly through the plane of the photographs and was aligned from the upper left to lower right of the picture. In this way, the expanding rings would rotate into the plane of the light sheet.

Of the approximately twenty sequences shot in this orientation, the best video sequence was obtained using an older apparatus, shown schematically in figure 7. The apparatus was constructed from sections of 7.62 cm PVC pipe fitted with sharp-edged orifices; inner diameters of the orifices were 5.82 cm. As in the previously described experiment, the generators faced each other so that their centrelines were parallel but offset in the horizontal plane. The offset distance was 2.54 cm and the distance between the orifices was 38.1 cm. Both generators were connected to a single driver through a symmetric arrangement of piping as shown in figure 7. The driver was simply a tube through which a puff of air was blown to displace water in the generators. Details of the experiment are presented in Smith (1992).

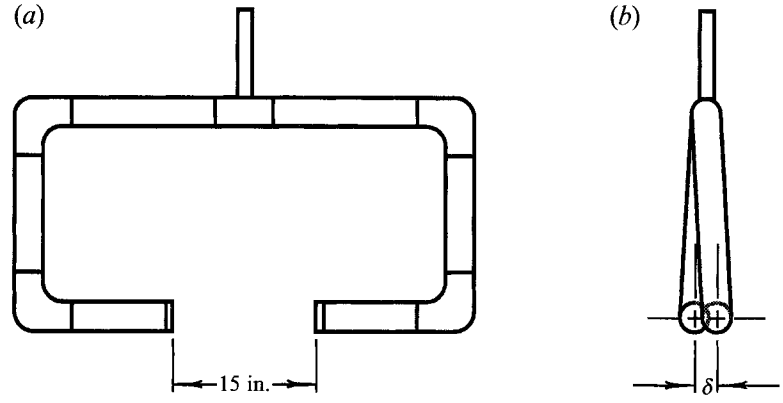

FIGURE 7. (a) Side- and (b) end-view orthographic projections of vortex generators used in the angled-laser-sheet visualization studies.

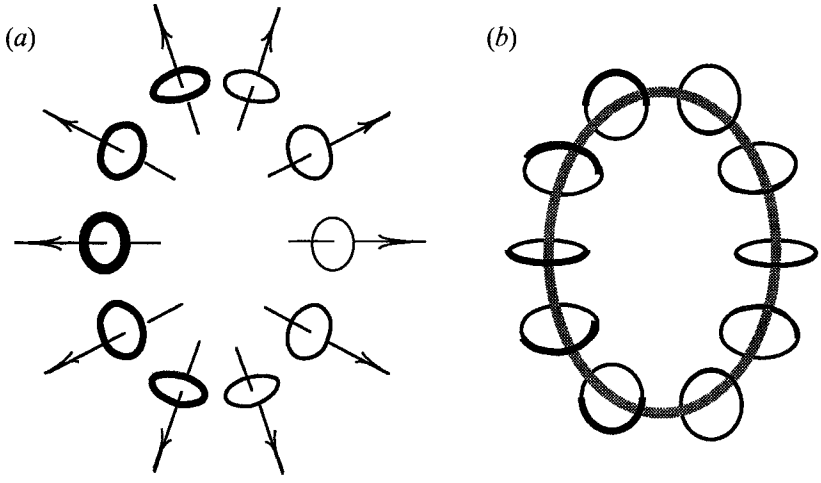

FIGURE 9. Schematic drawings highlighting the distinction between the ringlets in figure 8 and Lim & Nickels' (1992) small vortex rings: (a) the Lim & Nickels phenomenon; (b) an idealized sketch of the ringlets appearing in figure 8.

The advantage of this apparatus was its symmetry. It was possible to always generate two equal-strength vortex rings. The maximum deviation in Reynolds number between two rings in a colliding pair was found to be less than 2%. The disadvantage of the apparatus was that it was not possible to produce rings with a specific Reynolds number. The mean Reynolds number of the rings generated in this manner was 9300 with a standard deviation about the mean of ± 1330.

Figure 8 (plate 2), then, is a sequence of photographs taken from a run where a vertical laser sheet was aligned at $\sim 45°$ to the rings' propagation directions. Ring Reynolds numbers in this sequence were nominally 9300. There is 0.05 s between successive photographs. Counter to previous runs, figures 5 and 6, the red-marked ring approached from the right as the green-marked ring approached from the left.

The first photograph, figure 8(a), was taken just prior to the interaction. A portion of the green-marked ring is visible as the angled laser sheet hits one side of the ring. As time progresses the two rings expand and rotate into the plane of the laser sheet. Figures 8(b) and 8(c) show red dye beginning to appear around the edges of the green

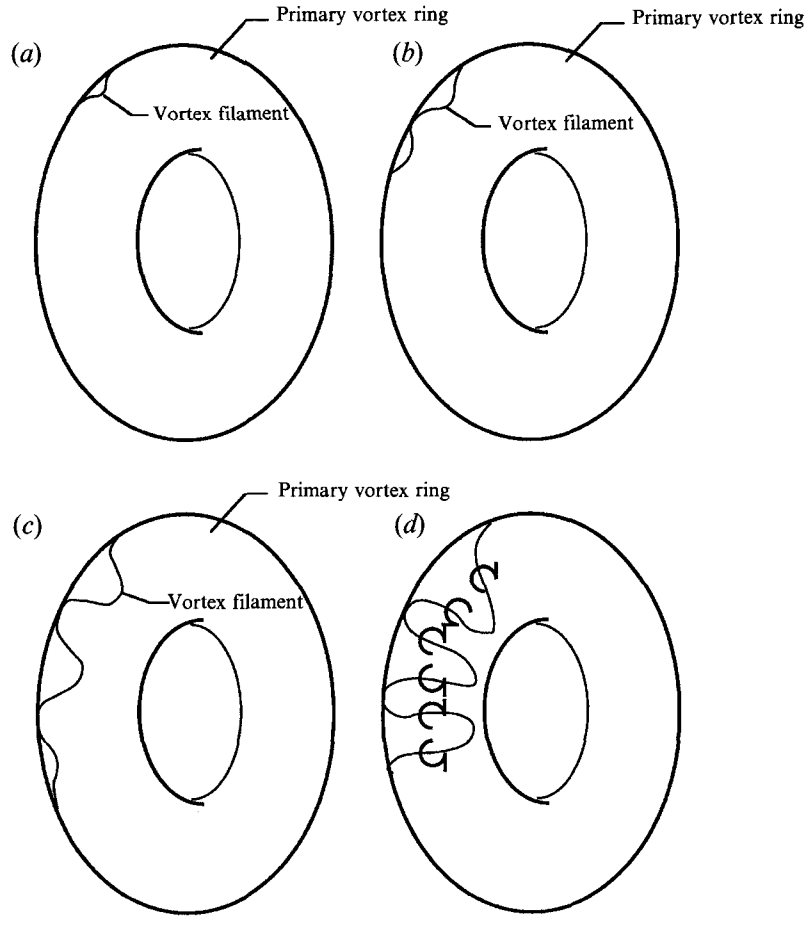

FIGURE 10. Schematic drawings highlighting the motion of wavy vortex lines across the surface of a primary vortex ring. Note how the wavy lines can lead to reorientation of vorticity into the counter-rotating ringlets seen in figure 8.

ring. Figures 8(*f–h*) show the formation of small rings around the original vortices. The entire structure breaks down to very small scales very soon after the last photograph.

There is a critical difference between the ringlets appearing in figure 8 and vortices described by Lim & Nickels (1992). This is illustrated in figure 9. Lim & Nickels' (1992) vortices, figure 9(*a*), propagate radially away from the symmetry axis. By contrast, ringlets formed during off-axis collisions, figure 9(*b*), appear to surround the primary vortex cores. This is not a simple rotation of the Lim & Nickels (1992) phenomenon.

One must conclude therefore, that ringlet formation is tied to the asymmetry of the primary ring collision; ringlets in figure 8 result from non-uniform vortex stretching of the primary rings. This can be seen by returning to figure 1. Along the vertical centreline, denoted Regions I, opposing vortex elements intersect. Primary rings actually collide here and may possibly reconnect. Opposing vortex elements at the outer edges of the interaction, however, are essentially parallel. These are denoted Regions II. It follows that Regions I will experience the greatest vortex stretching as well as the strongest amplification of ringlet-producing instabilities.

The nature of ringlet-producing instabilities is still an open question. One possibility

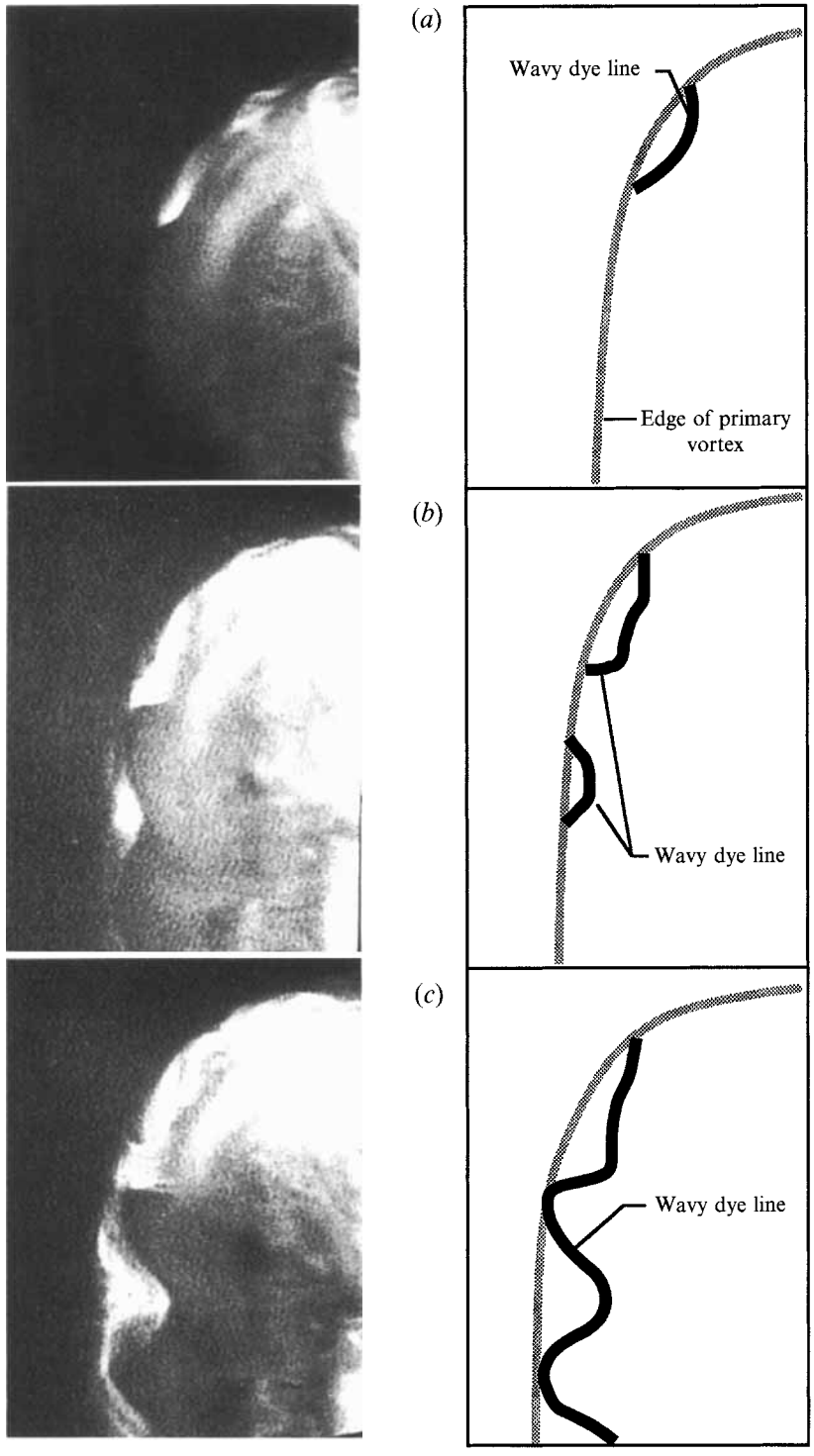

FIGURE 11. Oblique-view LIF sequence showing a close-up of ringlet formation. Wavy (green) dye lines move across the surface of a (green) primary vortex. Time between successive photographs is 0.0167 s.

is the Widnall instability which causes waviness of the primary vortex cores. In this scenario, opposing rings become wavy, intertwine, and reconnect to form ringlets. Another possibility is that waves form on the outer surfaces of the primary vortices while the cores remain essentially unaffected. This process, shown schematically in figure 10, is analogous to the helical vortex lines described by Lim (1989). In this case, non-uniform stretching of surface vorticity results in wavy vortex lines which wrap around the primary vortex cores to form ringlets.

Figure 10 shows four sketches of a wavy vortex line wrapping around the outside of a primary vortex ring. Figure 10(*a*) shows the peak of a single wave appearing in the upper left quadrant of the primary ring. Recall that this was designated as Region I in figure 1. Successive sketches illustrate increases in wave amplitude leading to formation of ringlets. As time progresses, waves move from the upper left quadrant toward the mid-plane of the primary ring, defined as Region II in figure 1. In figure 10(*d*), arrows indicate the direction of rotation of the wavy vortex line.

It is the opinion of the authors that the surface instability explanation is more likely. The most compelling evidence supporting this hypothesis appears in figure 11. This sequence shows a close-up of the early stages of ringlet formation corresponding to the upper left quadrant of figure 8; this sequence shows primarily the evolution of the green ring. Conditions were identical to those in figure 8. Time between successive photographs is 0.0167 s. By comparison, the time between photographs in figure 8 was 0.05 s; the total duration of the sequence in figure 11 is less than the time between two photographs in figure 8. Computer-assisted drawings showing amplification of surface waves are included for clarification.

The salient features in figure 11 are wavy dye lines passing over the surface of a (green) primary vortex. In figure 11(*a*), the crest of a single wave can be seen at the edge of the vortex ring in Region I (cf. figure 1). There is a strong similarity between figure 11(*a*) and the sketch in figure 10(*a*). In figures 11(*b*) and 11(*c*), waves can be seen wrapping around the surface of the primary ring into Region II (cf. figure 1). As pointed out in the previous paragraph, this is an extremely rapid process and would not be detectable in the photographs shown in figure 8; three times as many photographs would be required.

This wave propagation/amplification process reorients vorticity to produced counter-rotating ringlets as indicated in figure 10(*d*). Note that the primary vortex core does not exhibit any waviness throughout this process, as would be expected if the Widnall instability were excited. Based on these observations, it is believed that ringlet formation results from a process similar to that for helical vortex lines described by Lim (1989) and not from a primary vortex core instability like the Widnall instability.

4. Conclusions

An experimental investigation was conducted to examine off-axis collision of equal-strength vortex rings. Laser-induced-fluorescence flow visualization studies were used to examine small-scale motions resulting from the collision. Careful examination of the video records led to the following conclusions: (i) two colliding rings expand and rotate owing to induction of each ring on the other, and (ii) there is rapid formation of small ringlets which are believed to be vortices created by nonlinear amplification of instabilities in the primary vortex rings.

Support from NASA-Langley under Grant no. NGT-50707 is gratefully acknowledged.

REFERENCES

LIM, T. T. 1989 An experimental study of a vortex ring interacting with an inclined wall. *Exps Fluids* **7**, 453–463.

LIM, T. T. & NICKELS, T. B. Instability and reconnection in the head-on collision of two vortex rings. *Nature* **357**, 225–227.

SMITH, G. B. 1992 Turbulent cascade to small scales during the off-axis collision of two vortex rings. MS thesis, Dept of Mech. & Aero. Eng, Rutgers University.

SMITH, G. B. & WEI, T. 1991 Turbulent cascade in colliding off-axis vortex rings. *Bull. Am. Phys. Soc.* **36**, 2694.

ZAWADZKI, I. & AREF, H. 1991 Mixing during vortex ring collision. *Phys. Fluids* A3, 1405–1410.